Strengthening mechanisms in ultrafine grained Al-Mg-Si alloy processed by hydrostatic extrusion - influence of ageing temperature

Witold Chrominski[a], Sigurd Wenner[b], Calin D. Marioara[c], Randi Holmestad[b], Malgorzata Lewandowska[a]

[a]Faculty of Materials Science and Engineering, Warsaw University of Technology, Woloska 141, 02-507 Warsaw, Poland

[b] Department of Physics, Norwegian University of Science and Technology (NTNU), 7491 Trondheim, Norway

[c] SINTEF Materials and Chemistry, 7465 Trondheim, Norway

Corresponding author:

Witold Chrominski

Warsaw University of Technology

Faculty of Materials Science and Engineering

Woloska 141

02-507 Warsaw, POLAND

e-mail: wichr@inmat.pw.edu.pl

tel. +48-22-234-8441

fax. +48-22-234-8415

keywords: aluminium, ultrafine grained materials, precipitation strengthening, strengthening mechanisms, transmission electron microscopy

Abstract

Microstructure of hydrostatically extruded Al-Mg-Si alloy was studied by the combination of electron backscattered diffraction and transmission electron microscopy. Three different grain

types which feature various defects arrangements were detected. Post deformation ageing at two temperatures caused different precipitation phenomena which were strongly dependent on type of grain boundaries in the considered grain types. Thus, a combination of plastic deformation and ageing resulted in a material with complex microstructure. Based on transmission electron microscopy observations, contributions of different strengthening mechanisms were estimated and compared to experimental results. A good agreement between obtained data points confirmed that depending on grain type, different strengthening mechanisms are operative and the overall strength is a sum of hardening given by each of them. Ageing of ultrafine grain structure results in efficient precipitation strengthening. On the other hand ageing causes annihilation of low and high angle grains boundaries in which leads to softening of investigated material. This effect cannot be compensated by precipitation hardening.

1. Introduction

Ultrafine grained (UFG) materials processed by severe plastic deformation (SPD) techniques have been in the interest of the scientific community for over 20 years. The major strengthening mechanism acting in UFG materials is grain boundary strengthening, which links mechanical strength with the average grain size and assumes a homogenous microstructure. However, UFG materials are inherently inhomogeneous because the SPD techniques (like all plastic deformation processes) lead to microstructural heterogeneities. Grain refinement, in general, occurs via transformations of dislocation structures [1–3]. When dislocation cells reach their finest size, further plastic deformation causes dislocation cells rotations which result in an increase of misorientation angle between neighboring cells [3–5]. At a certain level of deformation, grain response to external stress occurs differently depending on its original orientation [6]. Thus, the process of grain refinement strongly

depends on the texture of a material. Even if very high strains are imposed with complex deformation routes a full homogenization of microstructure cannot be achieved [4,7,8]. One of the aspects of these heterogeneities is the fact that the fraction of high angle grain boundaries (HAGBs) typically saturates at 70% [4,8,9]. It means that the remaining 30% are low angle grain boundaries (LAGBs). The presence of HAGBs is a major strengthening factor, while LAGBs are not so efficient in these terms [16]. Another example of microstructure heterogeneity is grain size diversity, as well as the presence of various types of microstructures depending e.g. on local texture [10]. Local variations in microstructure can also influence precipitation processes in age hardenable alloys. The surface area of grain boundaries is significantly higher in UFG materials than in their conventional counterparts. It may change solute diffusion flux and alter precipitation processes. It has been shown that HAGBs attract solutes and serve as preferential nucleation sites for equilibrium precipitates without intermediate stages [11–13]. At the same time, this process reduces supersaturation of the grain interior which changes precipitation kinetics by increasing the nucleation energetic barrier. When final grains are relatively large, SPD does not change the precipitation sequence [14–18] but may influence size and spatial distribution of precipitates. However, in Ref. [19] a change in precipitation sequence has been noted for an Al-Mg-Si alloy due to diffusion of remaining alloying elements when main solutes had already formed early precipitates.

Al-Mg-Si alloys (6xxx series) are the most popular age hardenable aluminium alloys. Their mechanical properties combined with good corrosion resistance and satisfactory weldability make them a good choice in applications where mass should be reduced, like in the automotive industry. From a scientific point of view they are very interesting since the precipitation process is very complex and sensitive to pre-ageing treatment [20,21] as well as annealing conditions [22,23]. In general, the precipitation sequence in coarse grained

materials is relatively well described. It follows the order (phases present in Cu-containing alloys are given in parentheses):

supersaturated solid solution → Mg/Si co-clusters → GP zones → β`` (L) → β` + B` (Q`) → β [24–30]

This is a simplified sequence with indication of phases which are important in terms of this study. More detailed insight may by find in the cited papers.

The most desirable strengthening phases are β`` in non-Cu-containing and L in Cu-containing alloys [22,24,29]. It is related with strain fields caused by the coherency of these needle-like precipitates with the Al matrix [25,26,28,31]. The contribution of precipitates in Al-Mg-Si alloys into overall strength in coarse grained material was evaluated in Refs. [32–34]. It is clear from these studies that critical microstructure factors influencing mechanical properties are size and mean distance between precipitates. Hence, it is important to stop the ageing process when an optimal combination of these features is obtained.

In UFG materials, mechanical strength can be controlled by several mechanisms with grain boundary strengthening being the most prominent. Its efficiency depends on the mean distance between boundaries and their misorientation angle. The first empirical formalism of grain boundary strengthening mechanism was proposed by Hall and Petch [35,36] for materials with conventional grain size and simple microstructure. It was successfully applied to predict the influence of grain size on mechanical properties of UFG materials [37] with relatively uniform microstructure. This approach was extended by Hansen and his co-workers on cold rolled sheets containing very complex (but still one phase) microstructure with different types of dislocation arrangements [38,39]. This approach also includes crystallographic factors related with texture impact on dislocation slip.

In age hardenable alloys, it is possible to successfully combine precipitate and grain boundary strengthening to get even higher mechanical strength. Several papers report such a possibility

without any detailed microstructure investigations [15,16,40–42]. On the other hand, there are several works that evaluate different strengthening mechanisms with quantification of microstructure parameters [18,43–45]. It is shown there that in addition to grain boundary contribution, strength is also provided efficiently by precipitation processes in the grain interiors. Then the peak ageing condition can be reached faster and be stronger by adding these two mechanisms. However, a decrease of mechanical properties is rather caused by grain growth during long term annealing than changes in precipitation conditions. Other mechanisms like solid solution and dislocation strengthening are also present but their contribution is much smaller. Their sum gives the strengthening effect below 30% of overall strength in both cases as estimated in [18,43,44].

Most papers treat UFG materials as homogenous and when contributions of different strengthening mechanisms are evaluated it is assumed that they are equally effective in the entire volume of the investigated material. This is caused by necessary simplifications that are required by the physical models. However, microstructure in SPD processed metals is very complicated. It usually contains multiple texture components [46] and a network of high or low angle grain boundaries.

The novelty of this work is an attempt to estimate the contribution of different strengthening mechanisms taking into account the heterogeneity of the microstructure and its orientation dependence. To this end we selected hydrostatic extrusion (HE) as a processing technique because it provides an axially symmetric deformation which results in a sharp double fiber texture [10,47]. This allows us to quantify the microstructure more easily than in techniques producing more complex texture, for example equal channel angular pressing (ECAP).

2. Experimental

A commercially available 6082 Al-Mg-Si alloy with chemical composition (in weight %) of 0.79Mg-0.98Si-0.56Mn-0.24Fe-0.08Cu was supplied in the form of an extruded rod with a diameter of 50 mm in the T6 condition. Chemical composition was evaluated with a wavelength dispersive X-ray fluorescence spectrometer Bruker S4 Explorer. Billets for HE were solution heat treated in 520°C for 2h and quenched in cold water. Directly after quenching four stage HE was applied which resulted in a total accumulative strain of ε=4.6. Details of the HE technique and used procedure can be found in Ref. [12]. Every HE pass results in a temperature rise whose duration is reduced by a cooling system at the die exit. Although the temperature rise is reduced to a few seconds, it affects the microstructure by inducing early stages of precipitation as described in Ref. [19]. Such a material was then subjected to artificial ageing at 100 and 160°C for time periods within the range of 1-48h. These conditions were previously chosen according to hardness measurements in coarse grained samples. Mechanical properties of the UFG samples were measured by a tensile tests. Experiments were carried out with a MTS858 with an initial strain rate of 10^{-3}. Samples with a diameter of 2 mm and gauge length of 12 mm were used. Each value presented in this paper was averaged from three measurements.

Microstructure parameters for calculations were gathered mostly from TEM observations performed on thin discs taken from extruded and aged specimens. Electron transparent foils were obtained by conventional double sided electropolishing. A mixture of 2/3 methanol and 1/3 nitric acid cooled to approximately -25°C with a voltage of 20V was applied for thinning. Samples for electron backscatter diffraction (EBSD) measurements were electropolished in perchloric acid in ethanol (1:4). Additional ion polishing before observations was utilized if it was needed. EBSD analysis was performed on Hitachi SU-70 analytical scanning electron microscope with accelerating voltage of 20kV. Scans were done to extract texture data. Fractions of differently oriented grains were estimated by ratio of data points with specific

orientation to all properly resolved points. Scans were taken from a region of 125000 μm^2 to obtain good statistics.

Conventional TEM bright field imaging was done on a JEOL JEM 1200 EX II microscope with acceleration voltage 120kV. It was utilized to characterize deformation structures and quantify the fraction of refined grains as well as general precipitation observations. A simple stereological approach was used to estimate the volume fraction of regions which dimensions were too small to be detectable by EBSD. Volume fraction is given by $V_V = L_L$- ratio of length of test line intersections with a particular microstructure feature to the overall test line length [48]. Length of fine grains was measured along a specimen edge according to the assumption that the specimen thinning does not depend on microstructure. This approach is beneficial for two reasons: (i) no foil thickness determination is needed since on the edge line it can be neglected (ii) it significantly reduces the field of observations and does not require area quantification. The length of the specimen edges was measured in a Hitachi 5500S STEM. The grain size is expressed by equivalent diameter d_2 or surface area of boundaries per unit volume S_V. The relation between these parameters is $S_V = 2/d_2$ [38].

Precipitate density was determined using JEOL JEM 2100 TEM (operated at 200kV) equipped with an electron energy loss spectrometer (EELS) for determination of foil thickness (t) in the region of imaging. The grain of interest was tilted to its zone axis (in this study it was <001> see next section) and the EELS spectra was recorded with use of the direct beam in the diffraction pattern. The thickness was determined from inelastic electron mean free path, according to results taken from Ref. [49]. Such an approach gives the averaged value from the region which was selected by the diffraction aperture. Precipitates were found in grains with a cellular dislocation substructure. The size of the aperture was chosen to select only one particular subgrain. The number of precipitates was counted from the chosen region from bright field images with area A and divided by the volume of the region $V = At$ with t as

the specimen thickness. Precipitate density is expressed by a number per unit volume N_V or mean distance between them calculated from the doubled Wigner-Seitz radius [50]:

$$\lambda_p = 2\sqrt[3]{\frac{0.75}{\pi N_V}} \quad (1)$$

High resolution imaging, including high angle annular dark field scanning TEM (HAADF-STEM) imaging of precipitates for phase identification was done on a JEOL JEM 2100F TEM and a double corrected ARM-200F STEM, both operated at 200kV. Precipitates were identified by lattice periodicities and compared to available literature data.

3. Results

3.1 Grain types in the as-extruded material

Fig. 1(a) represents a {111} pole figure obtained by EBSD measurements performed on a cross section of the as-extruded material. Two concentric rings can be noticed and an agglomeration of data points in the central part of the pole figure. The rings indicate a double fiber texture with <001> and <111> fiber axes. Points in the center of the pole figure are related with <111> axis. The scattering of data points is quite narrow and thus the texture can be considered to be sharp. Measurements performed on inverse pole figures showed that deviation of fiber axes from a perfect orientation does not exceed 10° for both components. A detailed insight into the microstructure of differently oriented grains is given in Figs. 1 (b)-(d). One can see significant diffrences between the different grain types. A dislocation cellular structure is present in regions with <001> parallel to the extrusion direction (<001> grains). Cells interiors are mostly free from dislocations. This makes a benefitial condition for homogenous nucleation of early precipiates since no attraction of solutes occurs within subgrain interior nor to cell boundaries. Additionally the four thermal shocks preceding artificial ageing provide sufficent energy to start precipitation processes as reported in Refs [12,19]. Differences in shading level of each cell in Figs. 1 (b) are the result of slightly

different orientations but there are no sharp deviations between neighboring subgrains. Diffraction patterns taken from several neighboring cells idicate that they have a common [001] direction which is also the rotation axis. Diffraction spots are in the form of arcs indicating that cells rotate within the observed grain keeping constant axis. A mean misorientation angle of a particular dislocation wall is 1.5° as measured in EBSD. Texture data analysis revealed that the volume fraction of [001] grains is 22% and remains constant during further ageing process.

Two types of grains with <111> parallel to extrusion direction can be distinguished. They are shown in Fig.1 (c) and (d). The first type features non-homogenous amplitude contrast when imaged in bright field TEM. A tilting experiment revealed some dislocation boundaries by sharp changes in amplitude contrast between both sides of the boundary. EBSD data indicated that the average misorientation angle in regions with <111> parallel to the extrusion direction is 3°. In the rest of the text they will be referred to as <111> LA grains.

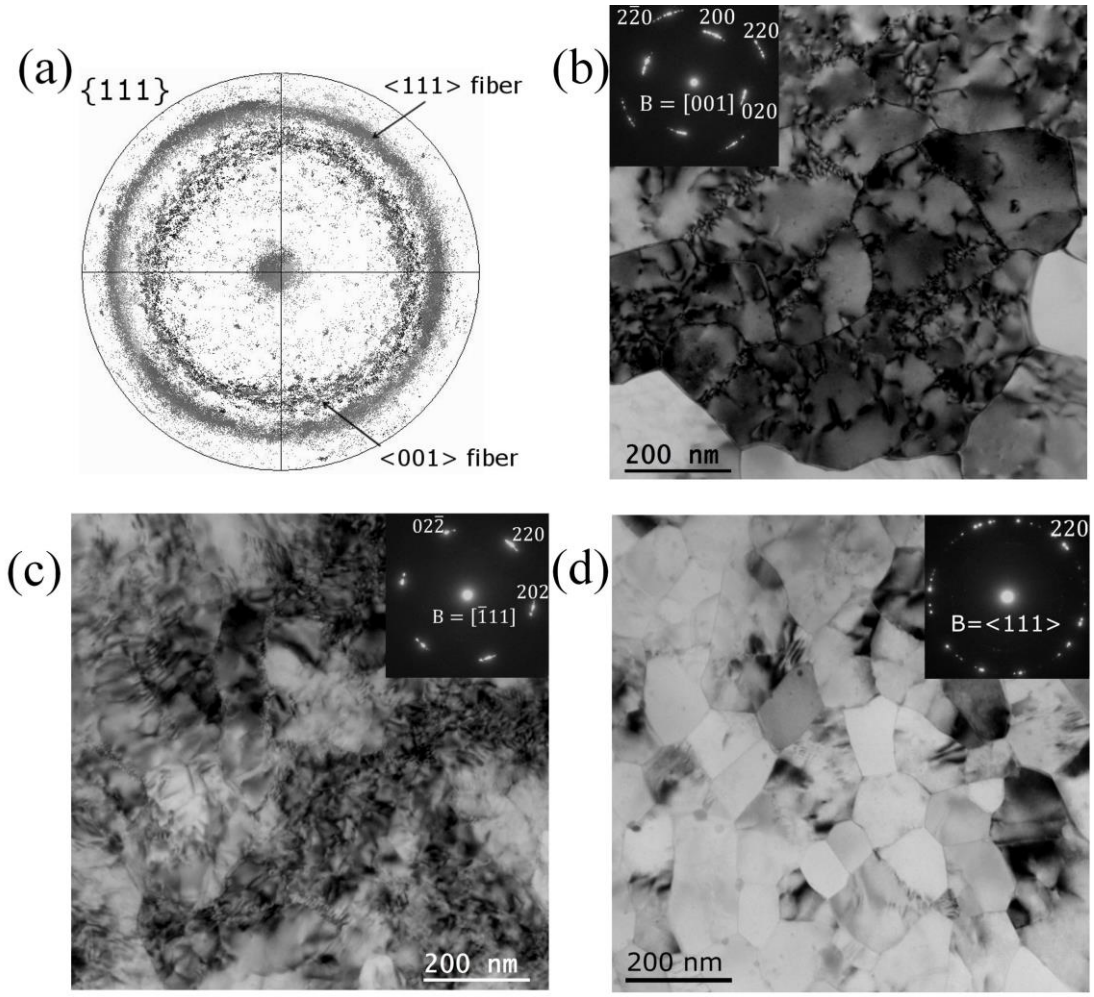

Fig. 1 Microstructure in the as-extruded condition (a) pole figure showing a strong double fiber texture, bright field images of typical (b) <001>, (c) <111> LA and (d) <111> HA grains, insets are diffraction patterns which allows to distinguish the different grain types

Analysis of diffraction patterns taken from the region in Fig.1 (c) showed that the rotation angle within considered area is lower than 15°. Thus, it can be concluded that this image contains few subgrains. From diffraction contrast experiments, no significant amount of dislocations between boundaries has been noticed. Then contrast changes in TEM images of this region are rather the result of strong internal stresses that cannot be accommodated by dislocation arrangements. No precipitation in the as-extruded condition nor in further ageing

was detected in such grains during TEM inspection of the samples. Thus it is concluded that all solutes remain solved in the matrix.

Fig.1 (d) shows the second type of grains with <111> parallel to extrusion direction. They are very fine (~130 nm) and well developed. No significant contrast heterogeneities nor dislocations within grain interiors were noticed during TEM investigations. The diffraction pattern (taken with the same aperture size as in the previous cases) consists of a ring formed by spots scattered on {220} planes. This suggests that rotations of grains occurred more efficiently than in other <111> regions and resulted in a dominance of high angle boundaries. Thus, it will be called <111> HA grains in the rest of the text. The total fraction of this grain type was estimated to 5% of all grains (detailed values are given in Section 3.3). This estimation was done in TEM, using the specimen edge measurement procedure described in the experimental part, since they were too fine to be detected in EBSD. Thus, the fraction of all types of <111> grains, which is the sum of <111>LA and <111>HA grains, is 78% (the rest is covered with <001> grains).

HAGBs are known to attract solutes which result in precipitation free zones (PFZs) covering the whole <111> HA grains. The enrichment of boundaries in solutes allows precipitates to be nucleated at preferential sites like triple points. This process is also facilitated by fast diffusion occurring along grain boundaries. As a result, grain boundaries are decorated with fine spherical Q`or Q precipitates [19] which reduce supersaturation in the interior of the <111> HA grains.

3.2 Precipitation

Precipitation phenomena have been reported only in <001> and <111> HA grains. In the former ones, the precipitates occur in the grain interior and can act as active obstacles for dislocation motion giving the strengthening effect. In the latter, the spherical phase nucleates

at triple points which reduces supersaturation and suppresses precipitation process in grain interiors. These occurrences are discussed in details in Refs. [12,19]. In the rest of the text, the precipitation in <001> grains is going to be discussed in detail since it gives a significant strengthening effect.

3.2.1 Ageing at 100℃

Several papers suggest that ageing of UFG materials should be performed at lower temperatures than the conventional material due to the accelerated diffusion [14,40,51]. Fig.2 shows precipitates in the alloy aged for 1h (a),(b) and 48h (c),(d). It can be noticed that precipitation does not change significantly between the two samples. In bright field images they appear as black spots homogenously distributed in the Al matrix. High resolution images show that they are fully coherent with the Al matrix and do not cause any significant distortion in the lattice periodicity. Even their diameter of 2 nm does not change with ageing time. According to the periodicity and the relation with matrix they are recognized as GP zones. Shape of GP zones is difficult to determine in TEM hence it is assumed that they are slightly elongated as revealed by APT studies [21,23,52]. Precipitates visible in Fig. 2 are the most likely aligned with the beam direction thus they appear in shape close to spherical. In Ref. [22] it was shown that in coarse grained material GP zones do not transform into the next phases below 125°C. In the light of this result it is concluded that in interior of <001> grains in UFG material precipitates follow the same tendency.

Fig.3 (a) illustrates a plot of precipitates density as a function of ageing time. It can be seen that even if GP zones do not evolve into next phases, their density is gradually increasing. This suggests that the process is controlled by slow volume diffusion and temperature is too low to induce a phase transformation of GP zones.

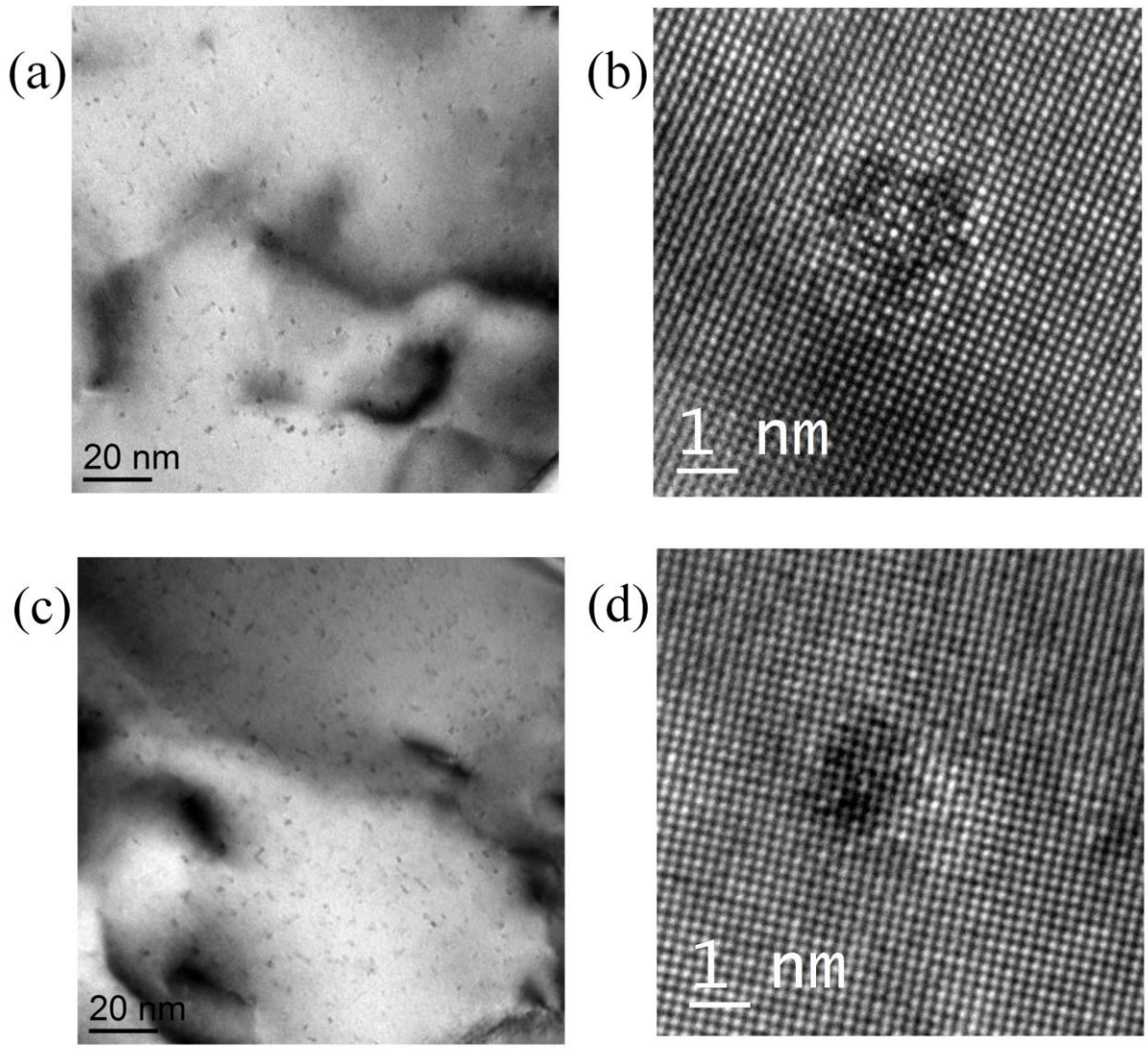

Fig. 2 Precipitation in <001> grains, aged in 100°C for 1h (a) bright field image showing high density of fine particles (b) HRTEM lattice image of GP zone and 48 h - (c) bright field image of fine particles similar to one observed for 1h ageing (d) HRTEM lattice image of GP zone

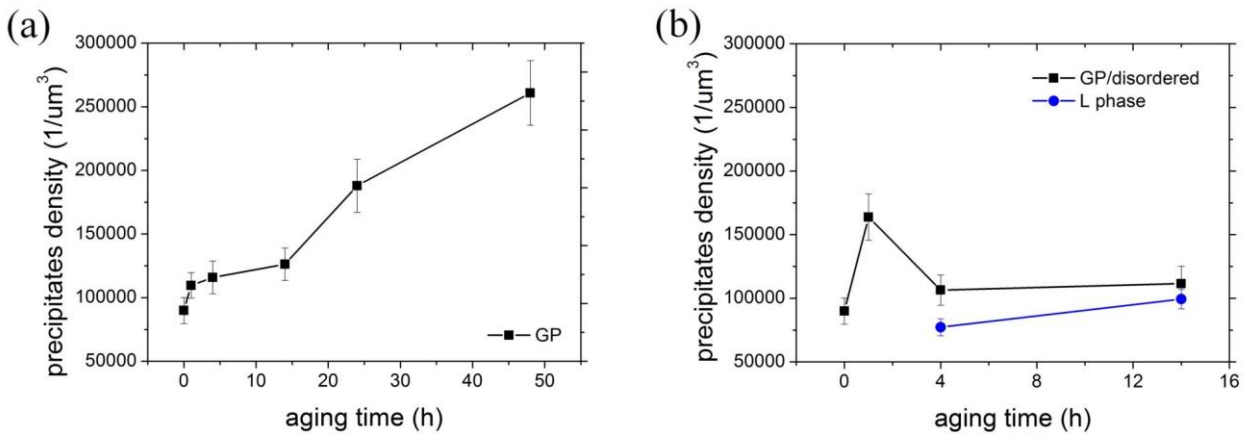

Fig. 3 Precipitate density in samples aged at (a) 100°C and (b) 160°C

3.2.2 Ageing at 160℃

Precipitates formed after 4 hours ageing at 160°C are depicted in Fig.4. One can see several needle shaped precipitates which long axis is aligned with three mutually perpendicular <001> type directions (Fig. 4(a)). Thus, one third of them are parallel to the viewing direction and visible as dark spots. For more detailed insight, a series of HR images were taken and three types of precipitates were identified depending on ageing time: (1) GP zones (Fig.4(b)) (2) L phase (Fig.4 (c), (d) and (e)) (3) random precipitates (Fig. 4(f)) .

Fig. 3(b) illustrates a plot of precipitate density as a function of ageing time. One can see that changes in precipitate density are much faster than at 100°C ageing due to accelerated diffusion. In particular, the density of fine precipitates increases rapidly after 1h ageing. Its decrease after ageing for 4 hours is caused by the phase transformation from GP zones into L phase precipitates according to the mechanism suggested in Ref. [19]. For 4 and 14 hours ageing random precipitates density remained constant as all GP zones have evolved into the L phase or dissolved due to thermal instability. The L phase does not change its density significantly even for longer ageing times.

Two most important phases in terms of precipitation strengthening are GP zones Fig.4 (b) and L phase precipitates, (c) and (d). The former are ellipsoidal-shaped and coherent with Al matrix. They serve as nucleation sites for needle shaped precipitates. GP zones are only present up to 4h ageing. After this, the small ones which could not serve as nucleation sites, become unstable and dissolve.

L phase needles appear after 4h ageing and their length grows from 13 to 17 nm after 14h. As can be seen in Fig. 4 (c) they can be hardly noticed in HRTEM when imaged edge-on due to coherency with the Al matrix. When the image is taken to reveal its cross section, a close to elliptical shape can be noticed. L phase is built by blocks of periodic structures which are aligned with <001>Al giving the precipitate a shape of a needle. Different structures and

possible precipitates in Al-Si-Mg alloys containing copper have been discussed in [53].Copper columns which define precipitate shape are marked on the STEM-HAADF image (Fig.4 (e)). The L phase density does not grow significantly up to 14h ageing.

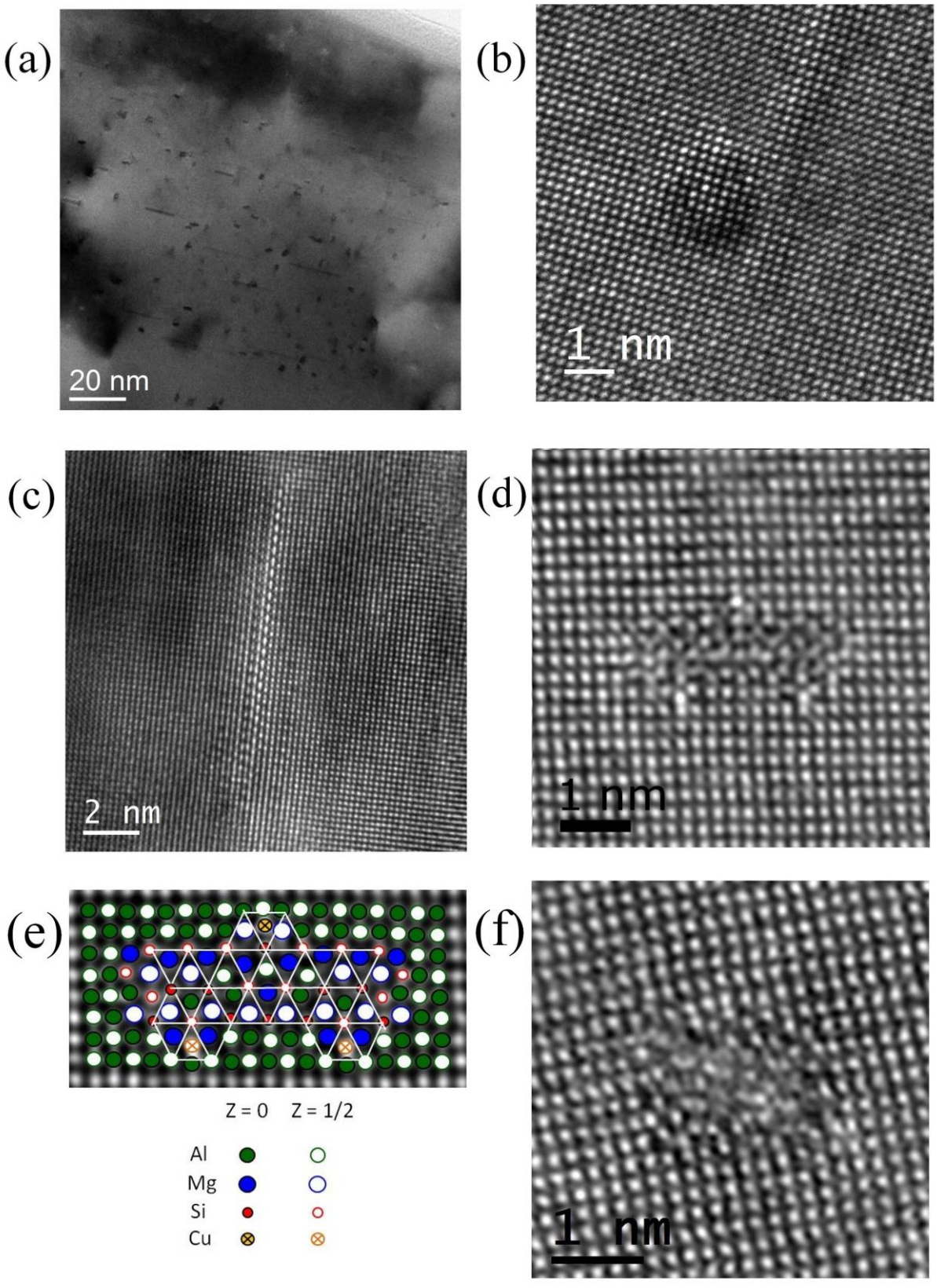

Fig. 4 Precipitation in <001> grains, for 4h ageing at 160°C (a) bright field of GP zones and needle shaped precipitates (b) HRTEM lattice image of GP zone (c) HRTEM lattice image of L phase (d) STEM-HAADF image of L phase cross section (e) suggested atomic overlay of L phase with indication of copper columns (f) STEM-HAADF image of a disordered precipitate

The last phase that may contribute to strengthening does not possess any evident symmetry so it cannot be identified. It is believed that this is a disordered phase which does not contain clearly developed crystal lattice [53]. Example of such a precipitate is shown in Fig.4 (f). They do not exhibit evident coherency with the Al matrix and when imaged in the [001] zone axis as no periodicity can be revealed. Thus, they are not believed to produce any coherency strain field but hinder dislocation motion as non-shearable precipitates.

3.2.3 Grain boundaries

Grain boundaries are known to alter precipitation phenomena due to easier diffusion. Additionally, boundaries attract solutes from their closest vicinity which deplete supersaturation and prevent nucleation and growth of precipitates in grain interiors. This results in PFZs formation. Efficiency of solute attraction depends on type of grain boundary. Dislocation boundaries in grains with <001> parallel to the extrusion direction attract solutes only from the closest ~10 nm [19]. However, this is enough to start the precipitation processes. Figs. 5 (a) and (b) show precipitates at dislocation boundaries in the material aged for 4h at 100 and 160°C, respectively. In the former one, very fine precipitates are present. They do not change with ageing time up to 48h. The latter shows fine needle shaped precipitates with their long direction aligned with $<100>_{Al}$.

Fig. 5 (c) shows a bright field image of spherical precipitates at grain boundaries in <111> HA grains. Such precipitates were found in the as-extruded condition and further ageing causes growth. They were recognized as close to equilibrium Q` phase or equilibrium Q. Mechanism of formation of such precipitates is suggested in Ref. [19]. Since HAGBs are more efficient in terms of solute attraction than LAGBs, the diffusion path in the former cover

whole grains. This inhibits precipitation inside grains and lowers the solute content in the matrix.

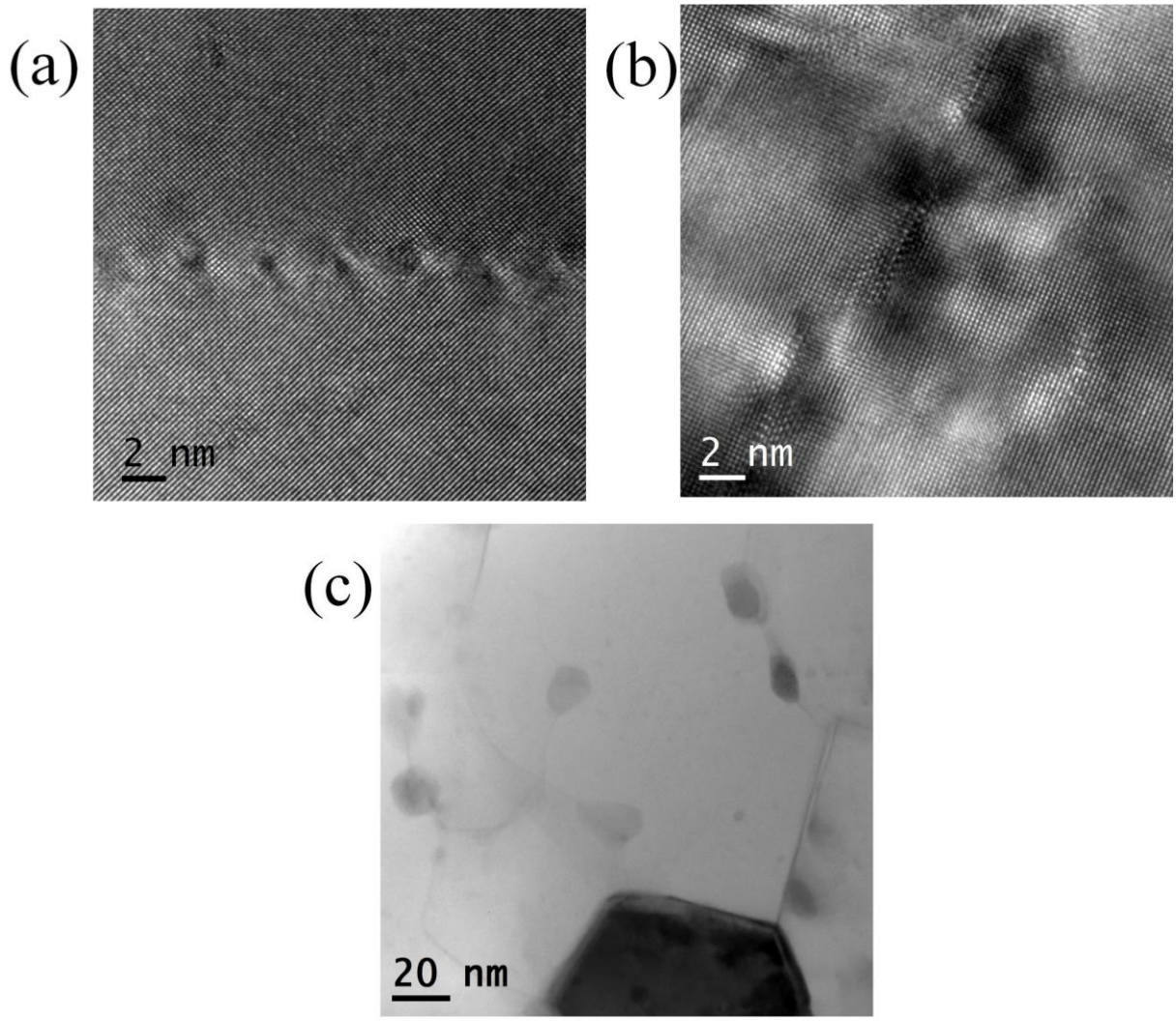

Fig. 5 Typical images of precipitation condition at grain boundaries (a) <001> grains, aged in 100°C for 4h (b) <001> grains, aged in 160° for 4h (c) <111> HA grains, aged in 100°C for 4h

3.3 Quantification of microstructure

Parameters necessary to estimate the contribution of different strengthening mechanisms to mechanical properties were gathered by TEM and EBSD investigations. As mentioned in Section 3.1, three different types of microstructure were detected in as-extruded and aged material. In order to estimate the fraction of each grain type, EBSD or the specimen edge measurement procedure described in the experimental section were utilized. In all further

calculations <001> grains are assumed to cover 22% of whole volume as this value was obtained from EBSD measurements of the investigated samples. The fraction of <111> HA grains changes with ageing conditions and is presented in Fig. 6 (a). Ageing at both temperatures causes a slight but clear decrease of the content of <111> HA grains. At the same time, their size increases. This effect is more pronounced for higher ageing temperature, as can be seen in Fig. 6 (b).

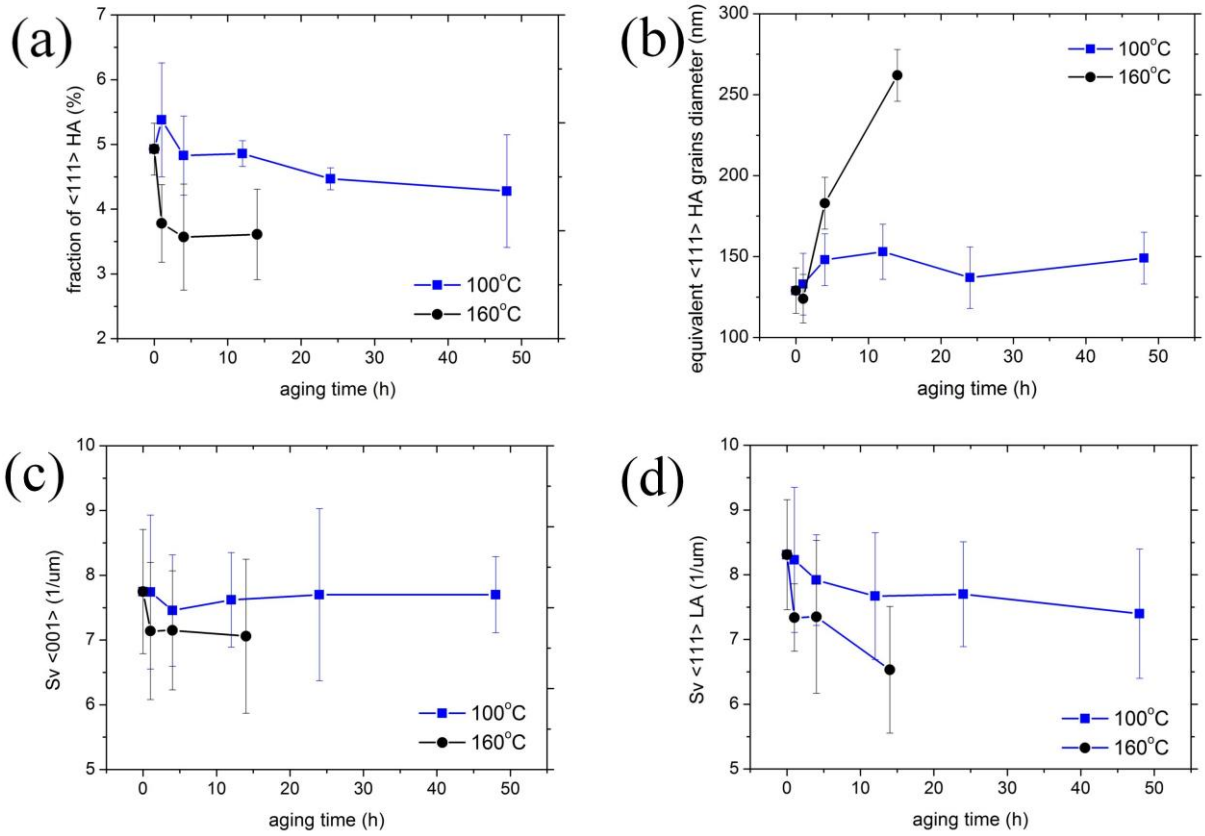

Fig. 6 Microstructure parameters measured for all ageing conditions (a) fraction of <111> HA grains (b) equivalent diameter of <111> HA grains (c) surface area of grain boundaries in <001> grains (d) surface area of grain boundaries in <111> LA grains

Figs. 6 (c) and (d) represent the plots of LAGB content expressed by S_V measured in fiber like <001> and <111> LA grains. Results were obtained from TEM observations close to perforation to minimize the effect of foil thickness. The behavior of dislocation boundaries is

slightly different for the two considered grain types. In <001> grains S_V value slightly decreases in the early ageing stages and then stabilizes at relatively constant level for both ageing temperatures. It should be noted that the higher temperature causes more intense decrease of LAGBs fraction during the first hours and stabilization of their contents occurs at lower level than in 100°C aged specimens.

In the case of <111> LA stabilization of dislocation boundaries during long term annealing did not occur. It results in a S_V drop which is more pronounced for 160°C. However, the general appearance of this grain type did not change even after 48h ageing and remains very similar to in the as-extruded condition (Fig.1 (c)).

4. Discussion

4.1 Microstructure evolution during ageing – operative strengthening mechanisms

Severe plastic deformation by HE and further heat treatment of extruded material results in a complex microstructure with several grain types with different operative strengthening mechanisms.

<111> HA grains are the most advanced grains in terms of the grain refinement process observed in the investigated samples. They feature diameter close to 130 nm (in the as-extruded condition) and are surrounded by HAGBs. All solutes dissolved inside them are assumed to be attracted by grain boundaries which resulted in precipitation of spherical particles close to triple points. Thus, these small grains are free from solutes and grain boundaries are responsible for the only strengthening mechanism. During ageing, the size of these grains increases and their volume fraction decreases (as depicted in Figs.6 (a) and (b)) which reduces their contribution in the overall strengthening effect. Spherical precipitates nucleate and grow at grain boundaries and cannot act as obstacles for dislocation motion. On

the other hand, they reduce solid solution strengthening by lowering the solute content in aluminium matrix.

<001> grains contain a dislocation boundary substructure and precipitates both in subgrain interiors and at boundaries. Dislocation walls provide strengthening by reducing the free path of mobile dislocations. The effect of ageing conditions on the surface area of subgrain boundaries is plotted in Fig. 6 (c). After an initial slight decrease, the S_V parameter stabilizes which can be caused by a pinning effect of very fine precipitates observed at dislocation boundaries for both ageing temperatures. Additional strengthening is provided by precipitation phenomena inside the subgrains. Type and density of precipitates depend on ageing conditions as depicted in Figs.2, 3 and 4.

<111> LA grains feature LAGBs and some dislocations between them. The surface area of these LAGBs significantly decreases with ageing time (Fig. 6 (d)) which can be attributed to the lack of precipitation phenomena in this grain type, as no stabilization of dislocation boundaries, as in <001> grains, occur. Two strengthening mechanisms are believed to be operative in such grains – by dislocation structures and solid solution strengthening. The latter was neglected in other grain types since precipitation phenomena were noticed which deplete the matrix from alloying elements. In <111> LA grains no precipitates were found thus all solutes must remain in the matrix.

Table 1 Parameters independent on material condition used to estimate strengthening mechanisms

symbol	value	physical meaning	reference
G	27 GPa	shearing modulus	
ν	0.33	Poisson ratio	
b	0.286 nm	magnitude of Burgers vector in Al	

σ_0	50 MPa	frictional stress of Al-Mg-Si alloys in Eqs. (3, 4)	[54]
k_y	0.326 MPa$\sqrt{\text{m}}$	Hall Petch slope in Eq. (3)	
α	0.24	constant in Eq. (4)	[39]
M_{001}	2.4	Taylor factor for <001> grains in Eq. (4, 5 and 6)	
M_{111}	3.25	Taylor factor for <111> grains in Eq. (4)	
β	0.28	constant related with dislocation line tension in Eq. (6)	[55]
k_{Mg}	29 $\frac{\text{MPa}}{\text{wt\%}^{2/3}}$	scaling factor for solid solution strengthening by Mg in Eq. (7)	[33]
k_{Si}	66.3$\frac{\text{MPa}}{\text{wt\%}^{2/3}}$	scaling factor for solid solution strengthening by Si in Eq. (7)	
k_{Cu}	46.4$\frac{\text{MPa}}{\text{wt\%}^{2/3}}$	scaling factor for solid solution strengthening by Cu in Eq. (7)	

4.2 Estimation of yield strength

Modeling of mechanical properties can be approached in several ways. Some microstructure oriented simulation methods take into account many materials factors and propose sophisticated equations which give a very good agreement with experimental data [56]. However, many parameters used in such studies cannot be easily measured due to limitation of experimental techniques. Thus, there is a need to simplify the models in studies involving experimental data by simple addition of the contribution of different strengthening mechanisms. Such simplifications also lead to satisfactory agreement between experimental

and theoretical values [18,32,33,43–45] and give a valuable insight into strengthening mechanisms based on microstructure observations.

In this study, we propose an additive approach supported by detailed microstructure investigations. It allows to attribute different strengthening mechanisms to different types of grains. The yield strength in the investigated material is a sum of lattice friction and strengthening effect given by different mechanisms which operate in different types of grains as described in the previous section. Thus, the strength given by each considered mechanism contributes according to the fraction of grains in which it is operative. This approach leads to the overall formula of:

$$\Delta\sigma = f_1\Delta\sigma_{HP} + f_2\Delta\sigma_{111} + f_3\Delta\sigma_{001} + f_4\Delta\sigma_{Or} + f_5\Delta\sigma_L + f_6\Delta\sigma_{ss} \quad (2)$$

Where: f_i is the fraction of grains with the particular operative strengthening mechanism - $f_{<001>} = 0.22$, $f_{<111>HA}$is taken from TEM observations, as provided in Fig. 6 (a), $f_{<111>LA} = 0.78 - f_{<111>HA}$:$\Delta\sigma_{HP}$ is the grain boundary strengthening from the Hall-Petch relationship in <111> HA grains, $\Delta\sigma_{111}$ is the strengthening from dislocation boundaries in <111> LA grains, $\Delta\sigma_{001}$ is the strengthening from dislocation structures in <001> grains, $\Delta\sigma_{\mathrm{Or}}$ is the strengthening by GP zones or random precipitates, $\Delta\sigma_{\mathrm{L}}$ is the strengthening by L phase and finally, $\Delta\sigma_{ss}$ is the solid solution strengthening.

Grain boundary strengthening is expressed by a well known Hall-Petch relationship [35,36]:

$$\Delta\sigma_{\mathrm{HP}} = \sigma_0 + \frac{\mathrm{k_y}}{\sqrt{\mathrm{d}}} \quad (3)$$

where: σ_0 - friction stress, $\mathrm{k_y}$ - Hall-Petch slope and d is a grain size. k_y depends on the material, however, a value of 0.326 MPa$\sqrt{\mathrm{m}}$ is used for Al-Mg-Si alloys [54]. This strengthening mechanism occurs only in <111> HA grains, therefore, to evaluate its contribution to overall strengthening, the volume fraction of such grains are taken from Fig. 6 (a).

Strengthening by incidental boundaries (dislocation boundaries with low misorientation angle) was identified in <001> and <111> LA grains and can be estimated using Hansen`s approach [38]. It was demonstrated that in materials with grain size in the UFG regime, strengthening effect from grain boundaries can be summed with those arising from incidental boundaries [63] according to Eq. (4):

$$\Delta\sigma_i = \sigma_0 + M_i \alpha G \sqrt{1.5 b S_V \frac{\pi\theta_i}{180}} \quad (4)$$

Eq. (4) was derived from the contribution of dislocations involved in incidental grain boundaries in overall dislocation density. Since this type of dislocation structures is the very early stage of new grain boundaries formation it causes only slight misorientation angle $\theta_i$between neighboring volume elements. In the materials investigated here, the nature of dislocation boundaries varies depending on grain orientation. Thus, the values of 1.5° and 3° were used for <001> and <111> LA grains, respectively, to calculate $\Delta\sigma_{001}$ and $\Delta\sigma_{111}$. They represent the mean misorientation angle within considered areas determined from EBSD measurements. Additionally, the values of the Taylor factor M_i with respect to grain orientation was used, as measured and discussed in [39].

To simplify calculations both GP zones and random precipitates present in <001> grains were considered as non-shearable spherical precipitates. GP zones possess the monoclinic unit cell [57] and random precipitates seem to feature no clearly developed lattice, as illustrated in Fig.4 (f). In all investigated conditions, their radius was close to 1 nm. According to this assumption they strengthen material via the Orowan looping mechanism. The strength provided by such particles is given by Eq. (5) [43]:

$$\Delta\sigma_{Or} = \frac{0.4 M_{001} G b}{\pi\sqrt{1-\nu}} \ln\left(\frac{2\bar{r}}{b}\right) \frac{1}{\lambda_p} \quad (5)$$

The distance between precipitates, λ_p, was calculated from their density with doubled Wigner-Seitz radius Eq.(1).

Needle-shaped precipitates are the most desirable ones in terms of mechanical strength in Al-Mg-Si alloys [24]. In the investigated material, the L phase was detected only in samples aged at 160°C for periods longer than 4h. The strengthening contribution of needle-shaped precipitates is calculated using Eq. (6) proposed and successfully applied by Bardel in Ref. [34] and later by Sauvage [18]:

$$\Delta\sigma_{\mathrm{L}} = 2\mathrm{M}_{001}\beta\mathrm{Gb}\frac{1}{\lambda} \quad (6)$$

It assumes that needle-shaped precipitates cannot be sheared by mobile dislocations and are bypassed when their radius is larger than 1.8 nm. The L phase possesses different lattice than Al with no repeating unit cell in their cross-sectional planes [29], thus the continuity of aluminium {111} slip planes in precipitates seems to be very unlikely. The average distance between these precipitates λ was calculated using their density similarly to GP zones or random precipitates.

According to the analysis in Section 4.1, solid solution strengthening operates only in <111> LA grains since no precipitation occurs in this grain type. Thus, such grains seem to remain in supersaturated solid solution condition. The influence of alloying elements to the overall strengthening effect can then be estimated by Eq. (7) [32,33]:

$$\Delta\sigma_{\mathrm{ss}} = \sum_{\mathrm{j}} \mathrm{k_j}\,\mathrm{C_j}^{2/3} \quad (7)$$

where: k_j is the scaling factor which values were experimentally measured in [33]. C_j is a concentration of alloying element in wt.%.

All constants and values independent of ageing conditions taken into the calculations are summarized in Table 1.

4.3 Contribution of different mechanisms to the overall strength of the material

Fig. 7 (a) represents a series of plots with yield strength estimated from our model, compared to experimental results obtained in tensile tests. It can be seen that estimated values follow the

same tendency as experimental data but do not match exactly the values from the experiment. This attributed to simplifications of the model which neglects for example free dislocation density, solutes other than Mg, Si and Cu and finally treats GP zone precipitates and the L phase separately. However, the values calculated are only estimations of the main operative strengthening mechanisms which, when sum up, give an estimation of yield strength. The accordance of main trends of calculated and experimental data points allows us to attribute changes of mechanical strength to the changes in operative strengthening mechanisms caused by ageing.

The plots of the strengthening effect of different mechanisms in samples aged in 100 and 160°C are shown in Figs. 7 (b) and (c), respectively. It can be seen that in both cases strength given by solutes dissolved in the matrix and dislocation structures in <001> grains remains at a relatively constant level for all ageing conditions. This is caused by no evident depletion of solutes in the former and stability of LAGBs in the latter.

The strengthening effect provided by grain boundaries (for both low and high angle ones) in <111> oriented regions slightly decreases with longer ageing times, as thermal stability of such structures is the weakest among all observed grain types, as described in Section 4.1. However, because of their fraction of about 70% in the microstructure, they provide the highest strength and are responsible for softening for longer ageing times. Thus, it can be stated that the final mechanical properties are strongly dependent on the microstructure in <111> oriented grains. At the same time when the fraction of grain boundaries in <111> grains decreases, nucleation and growth of the strengthening phases in <001> grains compensate the weakening of the material. In samples aged in 100°C, a constant increase of fine GP zones density provides monotonous growth of strength up to 48h. Softening in <111> grains is not intense enough to overpower this effect. This finally leads to continuous growth of mechanical properties during low temperature ageing.

Ageing at 160°C causes more complex precipitation phenomena with phase transformations, as presented in Section 3.2.2. Even if density of both precipitates types is lower than in 100°C ageing the combination of spherical precipitates and needle shaped L precipitates provide higher hardening of the material. It should be noted that precipitation strengthening accompanied with dislocation boundaries gives about 40% of total strength located within grain type which posses only 22% of volume. A decrease of mechanical properties after the peak aged condition is caused by the loss of grain boundary strengthening in <111> grains rather than a change in precipitation condition. It can be seen in Fig. 7 (c) that hardening from the L phase increases up to 14h, however, it is too low to compensate for grain boundary softening.

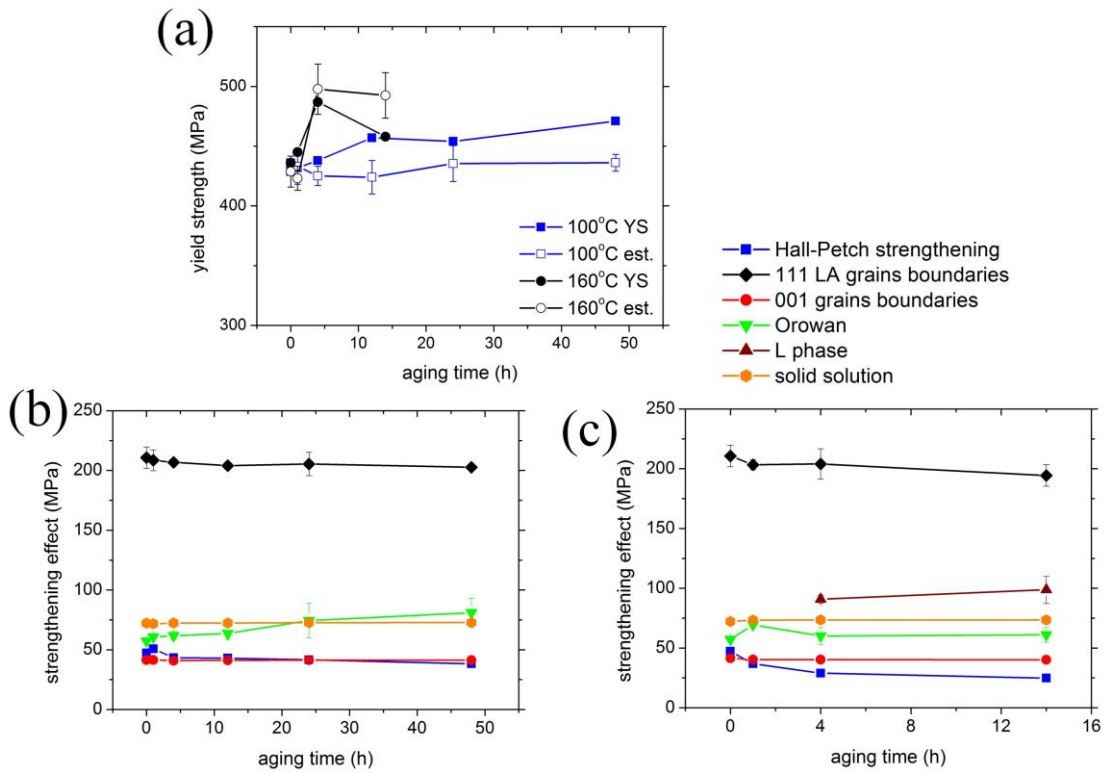

Fig. 7 Estimation of strengthening mechanisms in an ultrafine grained 6082 aluminium alloy subjected to ageing (a) comparison of yield strength measured in tensile test and value estimated from the model, contribution of different strengthening mechanisms in material aged in (b) 100°C (c) 160°C

5. Conclusions

Estimation of mechanical strength based on quantification of microstructure was done successfully and allowed us to compare contributions of different strengthening mechanisms in an ultrafine grained 6082 aluminium alloy after hydrostatic extrusion followed by conventional ageing. These investigations made us to conclude:

- Three various grain types have been found in the hydrostatically extruded aluminium alloy, these are the result of different stress conditions during plastic deformation. The substructure present in the particular grain types is responsible for the strengthening mechanism which is operative.
- The investigated material response acts differently on ageing in 100 and 160°C. In the former, monotonous growth of very fine spherical precipitates provides increase of mechanical strength up to 48h which is not compensated by softening caused by grain growth. In the latter, phase transformations of GP zones into L phase causes a large increase of hardening. At the same time random precipitates do not change their density and give an additional strengthening effect. However, a temperature of 160°C is high enough to produce grain growth which leads to mechanical weakening.
- Incidental grain boundaries in grains with <001> parallel to the extrusion direction do not change their size thanks to stabilization by very fine precipitates that occur during ageing.

Acknowledgements
This work was carried out within the statutory funds to the Faculty of Materials Science and Engineering of Warsaw University of Technology.
Furthermore, it is supported by the European Union in the framework of European Social Fund through the Warsaw University of Technology Development Programme, realized by Center for Advanced Studies.
SW, CDM and RH would like to thank the Research Council of Norway for funding through the FRINATEK project “Fundamental investigations of precipitation in the solid state with focus on Al-based alloys”. The JEOL JEM 2100F TEM and the double corrected ARM-200F are parts of the NORTEM infrastructure financed by the Research Council of Norway, NTNU and SINTEF.

References

[1] Y. Fukuda, K. Oh-ishi, M. Furukawa, Z. Horita, T.G. Langdon, The application of equal-channel angular pressing to an aluminum single crystal, Acta Mater. 52 (2004) 1387–1395. doi:10.1016/j.actamat.2003.11.028.
[2] Y. Iwahashi, Z. Horita, M. Nemoto, T.G. Langdon, The process of grain refinement in equal-channel angular pressing, Acta Mater. 46 (1998) 3317–3331. doi:10.1016/S1359-6454(97)00494-1.
[3] T.G. Langdon, The principles of grain refinement in equal-channel angular pressing, Mater. Sci. Eng. A. 462 (2007) 3–11. doi:10.1016/j.msea.2006.02.473.
[4] M. Cabibbo, E. Evangelista, C. Scalabroni, EBSD FEG-SEM, TEM and XRD techniques applied to grain study of a commercially pure 1200 aluminum subjected to equal-channel angular-pressing, Micron. 36 (2005) 401–414. doi:10.1016/j.micron.2005.03.004.
[5] M. Cabibbo, W. Blum, E. Evangelista, M.E. Kassner, M.A. Meyers, Transmission electron microscopy study of strain-induced low- and high-angle boundary development in equal-channel angular-pressed commercially pure aluminum, Metall. Mater. Trans. A. 39 (2008) 181–189. doi:10.1007/s11661-007-9350-z.
[6] Y. Fukuda, K. Oh-ishi, M. Furukawa, Z. Horita, T.G. Langdon, Influence of crystal orientation on ECAP of aluminum single crystals, Mater. Sci. Eng. A. 420 (2006) 79–86. doi:10.1016/j.msea.2006.01.086.
[7] M. Kawasaki, Z. Horita, T.G. Langdon, Microstructural evolution in high purity aluminum processed by ECAP, Mater. Sci. Eng. A. 524 (2009) 143–150. doi:10.1016/j.msea.2009.06.032.
[8] P.-L. Sun, P.-W. Kao, C.-P. Chang, Effect of deformation route on microstructural development in aluminum processed by equal channel angular extrusion, Metall. Mater. Trans. A. 35 (2004) 1359–1368. doi:10.1007/s11661-004-0311-5.
[9] P.B. Prangnell, J.R. Bowen, P.J. Apps, Ultra-fine grain structures in aluminium alloys by severe deformation processing, Mater. Sci. Eng. A. 375-377 (2004) 178–185. doi:10.1016/j.msea.2003.10.170.
[10] W. Chrominski, M. Lewandowska, Dislocation Substructure Evolution during Hydrostatic Extrusion of Al Mg Si Alloy, Acta Phys. Pol. A. 128 (2015) 585–588. doi:10.12693/APhysPolA.128.585.
[11] T. Hu, K. Ma, T.D. Topping, J.M. Schoenung, E.J. Lavernia, Precipitation phenomena in an ultrafine-grained Al alloy, Acta Mater. 61 (2013) 2163–2178. doi:10.1016/j.actamat.2012.12.037.
[12] W. Chrominski, M. Kulczyk, M. Lewandowska, K.J. Kurzydlowski, Precipitation strengthening of ultrafine-grained Al-Mg-Si alloy processed by hydrostatic extrusion, Mater. Sci. Eng. A. 609 (2014) 80–87. doi:10.1016/j.msea.2014.04.092.
[13] Y. Huang, J.D. Robson, P.B. Prangnell, The formation of nanograin structures and accelerated room-temperature theta precipitation in a severely deformed Al-4 wt.% Cu alloy, Acta Mater. 58 (2010) 1643–1657. doi:10.1016/j.actamat.2009.11.008.
[14] M. Hockauf, L.W. Meyer, B. Zillmann, M. Hietschold, S. Schulze, L. Krüger, Simultaneous improvement of strength and ductility of Al-Mg-Si alloys by combining equal-channel angular extrusion with subsequent high-temperature short-time aging, Mater. Sci. Eng. A. 503 (2009) 167–171. doi:10.1016/j.msea.2008.02.051.
[15] Y.H. Zhao, X.Z. Liao, Z. Jin, R.Z. Valiev, Y.T. Zhu, Microstructures and mechanical properties of ultrafine grained 7075 Al alloy processed by ECAP and their evolutions during annealing, Acta Mater. 52 (2004) 4589–4599. doi:10.1016/j.actamat.2004.06.017.
[16] M.H. Li, Y.Q. Yang, Z.Q. Feng, G.H. Feng, B. Huang, Y.X. Chen, et al., Influence of equal-channel angular pressing on aging precipitation in 7050 Al alloy, Intermetallics.

55 (2014) 49–55. doi:10.1016/j.intermet.2014.07.005.
[17] M. Murayama, Z. Horita, K. Hono, Microstructure of two-phase Al – 1.7 at % Cu alloy deformed by equal-channel angular pressing, Acta Mater. 49 (2001) 21–29. http://www.sciencedirect.com/science/article/B6TW8-424KW36-4/2/50282b1d9c56c605d5b54778d90cacb7.
[18] X. Sauvage, E. V Bobruk, M.Y. Murashkin, Y. Nasedkina, N.A. Enikeev, R.Z. Valiev, Optimization of electrical conductivity and strength combination by structure design at the nanoscale in Al – Mg – Si alloys, Acta Mater. 98 (2015) 355–366. doi:10.1016/j.actamat.2015.07.039.
[19] W. Chrominski, M. Lewandowska, Precipitation phenomena in ultrafine grained Al–Mg–Si alloy with heterogeneous microstructure, Acta Mater. 103 (2016) 547–557. doi:10.1016/j.actamat.2015.10.030.
[20] K. Matsuda, H. Gamada, Y. Uetani, S. Rengakuji, F. Shinagawa, S. Ikeno, Specific precipitates in Al-Mg2Si alloys aged after deformation, J. Japan Inst. Light Met. 48 (1998) 471–475.
[21] M. Murayama, K. Hono, Pre-precipitate clusters and precipitation processes in Al-Mg-Si alloys, Acta Mater. 47 (1999) 1537–1548. doi:10.1016/S1359-6454(99)00033-6.
[22] C.D. Marioara, S.J. Andersen, J. Jansen, H.W. Zandbergen, The influence of temperature and storage time at RT on nucleation of the β`` phase in a 6082 Al-Mg-Si alloy, Acta Mater. 51 (2003) 789–796. doi:10.1016/S1359-6454(02)00470-6.
[23] S. Pogatscher, H. Antrekowitsch, H. Leitner, A.S. Sologubenko, P.J. Uggowitzer, Influence of the thermal route on the peak-aged microstructures in an Al-Mg-Si aluminum alloy, Scripta Mater. 68 (2013) 158–161. doi:10.1016/j.scriptamat.2012.10.006.
[24] G.A. Edwards, K. Stiller, G.L. Dunlop, M.J. Couper, The precipitation sequence in Al–Mg–Si alloys, Acta Mater. 46 (1998) 3893–3904. doi:10.1016/S1359-6454(98)00059-7.
[25] W. Yang, L. Huang, R. Zhang, M. Wang, Z. Li, Y. Jia, et al., Electron microscopy studies of the age-hardening behaviors in 6005A alloy and microstructural characterizations of precipitates, J. Alloys Compd. 514 (2012) 220–233. doi:10.1016/j.jallcom.2011.11.074.
[26] T. Saito, C.D. Marioara, S.J. Andersen, W. Lefebvre, R. Holmestad, Aberration-corrected HAADF-STEM investigations of precipitate structures in Al–Mg–Si alloys with low Cu additions, Philos. Mag. 94 (2013) 520–531. doi:10.1080/14786435.2013.857051.
[27] C.D. Marioara, H. Nordmark, S.J. Andersen, R. Holmestad, Post-β`` phases and their influence on microstructure and hardness in 6xxx Al-Mg-Si alloys, J. Mater. Sci. 41 (2006) 471–478. doi:10.1007/s10853-005-2470-1.
[28] W. Yang, S. Ji, L. Huang, X. Sheng, Z. Li, M. Wang, Initial precipitation and hardening mechanism during non-isothermal aging in an Al–Mg–Si–Cu 6005A alloy, Mater. Charact. 94 (2014) 170–177. doi:10.1016/j.matchar.2014.05.007.
[29] C.D. Marioara, S.J. Andersen, T.N. Stene, H. Hasting, J. Walmsley, A.T.J. Van Helvoort, et al., The effect of Cu on precipitation in Al–Mg–Si alloys, Philos. Mag. 87 (2007) 3385–3413. doi:10.1080/14786430701287377.
[30] M. Liu, J. Čížek, C.S.T. Chang, J. Banhart, Early stages of solute clustering in an Al–Mg–Si alloy, Acta Mater. 91 (2015) 355–364. doi:10.1016/j.actamat.2015.02.019.
[31] P.H. Ninive, A. Strandlie, S. Gulbrandsen-Dahl, W. Lefebvre, C.D. Marioara, S.J. Andersen, et al., Detailed atomistic insight into the β″ phase in Al-Mg-Si alloys, Acta Mater. 69 (2014) 126–134. doi:10.1016/j.actamat.2014.01.052.
[32] O.R. Myhr, Ø. Grong, Modelling of the microstructure and strength evolution in Al –

Mg – Si alloys during multistage thermal processing, Acta Mater. 52 (2004) 4997–5008. doi:10.1016/j.actamat.2004.07.002.
[33] O.R. Myhr, Ø. Grong, S.J. Andersen, Modelling of the age hardening behaviour of Al-Mg-Si alloys, Acta Mater. 49 (2001) 65–75.
[34] D. Bardel, M. Perez, D. Nelias, A. Deschamps, C.R. Hutchinson, Coupled precipitation and yield strength modelling for non-isothermal treatments of a 6061 aluminium alloy, Acta Mater. 62 (2014) 129–140. doi:10.1016/j.actamat.2013.09.041.
[35] E.O. Hall, The Deformation and Ageing of Mild Steel: III Discussion of Results, Preceedings Phys. Soc. Sect. B. 64 (1951) 747–753.
[36] N.J. Petch, The cleavage strengtth of polycrystals, J Iron Steel Inst. 19 (1953) 25–28.
[37] M.A. Meyers, A. Mishra, D.J. Benson, Mechanical properties of nanocrystalline materials, Prog. Mater. Sci. 51 (2006) 427–556. doi:10.1016/j.pmatsci.2005.08.003.
[38] D.A. Hughes, N. Hansen, Microstructure and strength of nickel at large strains, Acta Mater. 48 (2000) 2985–3004.
[39] N. Hansen, X. Huang, Microstructure and flow stress of polycrystals and single crystals, Acta Metall. 46 (1998) 1827–1836.
[40] M. Vaseghi, H.S. Kim, A combination of severe plastic deformation and ageing phenomena in Al-Mg-Si Alloys, Mater. Des. 36 (2012) 735–740. doi:10.1016/j.matdes.2011.12.014.
[41] K. Hockauf, L.W. Meyer, M. Hockauf, T. Halle, Improvement of strength and ductility for a 6056 aluminum alloy achieved by a combination of equal-channel angular pressing and aging treatment, J. Mater. Sci. 45 (2010) 4754–4760. doi:10.1007/s10853-010-4544-y.
[42] J.K. Kim, H.G. Jeong, S.I. Hong, Y.S. Kim, W.J. Kim, Effect of aging treatment on heavily deformed microstructure of a 6061 aluminum alloy after equal channel angular pressing, Scripta Mater. 45 (2001) 901–907. doi:10.1016/S1359-6462(01)01109-5.
[43] K. Ma, H. Wen, T. Hu, T.D. Topping, D. Isheim, D.N. Seidman, et al., Mechanical behavior and strengthening mechanisms in ultrafine grain precipitation-strengthened aluminum alloy, Acta Mater. 62 (2014) 141–155. doi:10.1016/j.actamat.2013.09.042.
[44] P.N. Rao, D. Singh, H.-G. Brokmeier, R. Jayaganthan, Effect of ageing on tensile behavior of ultrafine grained Al 6061 alloy, Mater. Sci. Eng. A. 641 (2015) 391–401. doi:10.1179/174328409X443227.
[45] Y. Chen, N. Gao, G. Sha, S.P. Ringer, M.J. Starink, Microstructural evolution , strengthening and thermal stability of an ultra fi ne-grained Al e Cu e Mg alloy, Acta Mater. 109 (2016) 202–212. doi:10.1016/j.actamat.2016.02.050.
[46] I.J. Beyerlein, L.S. Tóth, Progress in Materials Science Texture evolution in equal-channel angular extrusion, Prog. Mater. Sci. 54 (2009) 427–510. doi:10.1016/j.pmatsci.2009.01.001.
[47] M. Lewandowska, Mechanism of Grain Refinement in Aluminium in the Process of Hydrostatic Extrusion, Solid State Phenom. 114 (2006) 109–116. doi:10.4028/www.scientific.net/SSP.114.109.
[48] J.C. Russ, R.T. Dehoff, Practical Stereology, 1999.
[49] K. Iakoubovskii, K. Mitsuishi, Y. Nakayama, K. Furuya, Mean free path of inelastic electron scattering in elemental solids and oxides using transmission electron microscopy: Atomic number dependent oscillatory behavior, Phys. Reviev B. 77 (2008) 1–7. doi:10.1103/PhysRevB.77.104102.
[50] L.A. Girifalco, Statistical mechanics of solids, 2000.
[51] A. Deschamps, F. De Geuser, Z. Horita, S. Lee, G. Renou, Precipitation kinetics in a severely plastically deformed 7075 aluminium alloy, Acta Mater. 66 (2014) 105–117. doi:10.1016/j.actamat.2013.11.071.

[52] M.W. Zandbergen, Q. Xu, a. Cerezo, G.D.W. Smith, Study of precipitation in Al–Mg–Si alloys by Atom Probe Tomography I. Microstructural changes as a function of ageing temperature, Acta Mater. 101 (2015) 136–148. doi:10.1016/j.actamat.2015.08.017.
[53] F.J.H. Ehlers, S. Wenner, S.J. Andersen, C.D. Marioara, W. Lefebvre, C.B. Boothroyd, et al., Phase stabilization principle and precipitate-host lattice influences for Al – Mg – Si – Cu alloy precipitates, J. Mater. Sci. (2014) 6413–6426. doi:10.1007/s10853-014-8371-4.
[54] A. Loucif, R.B. Figueiredo, T. Baudin, R. Chemam, T.G. Langdon, Ultrafine grains and the Hall – Petch relationship in an Al – Mg – Si alloy processed by high-pressure torsion, Mater. Sci. Eng. A. 532 (2012) 139–145. doi:10.1016/j.msea.2011.10.074.
[55] C. Gallais, A. Denquin, Y. Bréchet, G. Lapasset, Precipitation microstructures in an AA6056 aluminium alloy after friction stir welding : Characterisation and modelling, Mater. Sci. Eng. A. 496 (2008) 77–89. doi:10.1016/j.msea.2008.06.033.
[56] A. De Vaucorbeil, W.J. Poole, C.W. Sinclair, Materials Science & Engineering A The superposition of strengthening contributions in engineering alloys, Mater. Sci. Eng. A. 582 (2013) 147–154. doi:10.1016/j.msea.2013.06.032.
[57] C.D. Marioara, S.J. Andersen, J. Jansen, H.W. Zandbergen, Atomic model for GP-zones in a 6082 Al-Mg-Si system, Acta Mater. 49 (2001) 321–328. doi:10.1016/S1359-6454(00)00302-5.